HHS Public Access

Author manuscript

Acta Biomater. Author manuscript; available in PMC 2016 May 01.

Published in final edited form as:

Acta Biomater. 2015 May ; 18: 236–248. doi:10.1016/j.actbio.2015.02.011.

Bone tissue engineering via human induced pluripotent, umbilical cord and bone marrow mesenchymal stem cells in rat cranium

Ping Wang[a,b], **Xian Liu**[a,b], **Liang Zhao**[a,c], **Michael D. Weir**[a], **Jirun Sun**[d], **Wenchuan Chen**[a,b], **Yi Man**[b], and **Hockin H. K. Xu**[a,e,f,g]

[a] Biomaterials & Tissue Engineering Division, Department of Endodontics, Prosthodontics and Operative Dentistry, University of Maryland Dental School, Baltimore, MD 21201, USA

[b] State Key Laboratory of Oral Diseases, West China Hospital of Stomatology, Sichuan University, Chengdu, Sichuan 610041, China

[c] Department of Orthopaedic Surgery, Nanfang Hospital, Southern Medical University, Guangzhou, Guangdong 510515, China

[d] Dr. Anthony Volpe Research Center, American Dental Association Foundation, Gaithersburg, MD 20899, USA

[e] Center for Stem Cell Biology and Regenerative Medicine, University of Maryland School of Medicine, Baltimore, MD 21201, USA

[f] University of Maryland Marlene and Stewart Greenebaum Cancer Center, University of Maryland School of Medicine, Baltimore, MD 21201, USA

[g] Mechanical Engineering Department, University of Maryland Baltimore County, Baltimore, MD 21250, USA

Abstract

Human induced pluripotent stem cells (hiPSCs) are an exciting cell source with great potential for tissue engineering. Human bone marrow mesenchymal stem cells (hBMSCs) have been used in clinics but are limited by several disadvantages, hence alternative sources of MSCs such as umbilical cord MSCs (hUCMSCs) are being investigated. However, there has been no report comparing hiPSCs, hUCMSCs and hBMSCs for bone regeneration. The objectives of this pilot study were to investigate hiPSCs, hUCMSCs and hBMSCs for bone tissue engineering, and compare their bone regeneration via seeding on biofunctionalized macroporous calcium phosphate

Correspondence: Dr. Hockin H. K. Xu, Professor, Director of Biomaterials & Tissue Engineering Division, Department of Endodontics, Prosthodontics and Operative Dentistry, University of Maryland Dental School, Baltimore, MD 21201 (hxu@umaryland.edu). Dr. Liang Zhao, Department of Orthopaedic Surgery, Nanfang Hospital, Southern Medical University, Guangzhou, Guangdong 510515, China (lzhaonf@126.com)..

Conflict of interest

None.

cement (CPC) in rat cranial defects. For all three types of cells, approximately 90% of the cells remained alive on CPC scaffolds. Osteogenic genes were up-regulated, and mineral synthesis by cells increased with time *in vitro* for all three types of cells. The new bone area fractions at 12 weeks (mean ± sd; n = 6) were (30.4 ± 5.8)%, (27.4 ± 9.7)% and (22.6 ± 4.7)% in hiPSC-MSC-CPC, hUCMSC-CPC and hBMSC-CPC respectively, compared to (11.0 ± 6.3)% for control ($p < 0.05$). No significant differences were detected among the three types of stem cells ($p > 0.1$). New blood vessel density was higher in cell-seeded groups than control ($p < 0.05$). *De novo* bone formation and participation by implanted cells was confirmed via immunohistochemical staining. In conclusion, (1) hiPSCs, hUCMSCs and hBMSCs greatly enhanced bone regeneration, more than doubling the new bone amount of cell-free CPC control; (2) hiPSC-MSCs and hUCMSCs represented viable alternatives to hBMSCs; (3) biofunctionalized macroporous CPC-stem cell constructs had a robust capacity for bone regeneration.

Graphical Abstract

Human induced pluripotent stem cells (hiPSCs) are an exciting cell source with great potential for tissue engineering. Human bone marrow mesenchymal stem cells (hBMSCs) are used in clinics but are limited by several disadvantages. Alternative sources of MSCs, such as umbilical cord MSCs (hUCMSCs), are being investigated. However, there has been no report comparing hiPSCs, hUCMSCs and hBMSCs for bone regeneration in vivo. This study investigated hiPSCs, hUCMSCs and hBMSCs in biofunctionalized macroporous calcium phosphate cement (CPC) scaffolds in rat cranial defects for the first time. At 12 weeks, new bone area fraction of hiPSC-MSC-CPC was (30.4 ± 5.8)%, 2.8-fold that of cell-free CPC control. Seeding with hiPSCs, hUCMSCs and hBMSCs in CPC greatly enhanced bone regeneration. Therefore, hiPSC-MSCs and hUCMSCs represented viable alternatives to hBMSCs, and biofunctionalized macroporous CPC was suitable for stem cell delivery and bone regeneration.

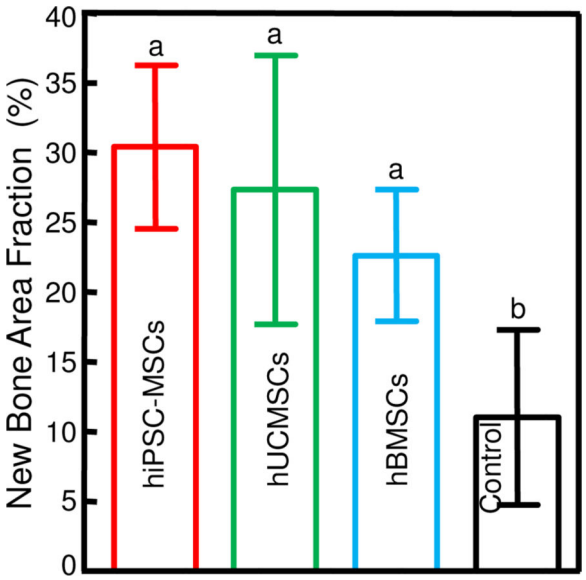

Keywords

Induced pluripotent stem cells; umbilical cord stem cells; bone marrow stem cells; calcium phosphate scaffold; bone regeneration

1. Introduction

In the field of bone tissue engineering and regenerative medicine, generating patient-specific stem cells has been a long-standing goal [1-3]. Human bone marrow mesenchymal stem cells (hBMSCs) are the current gold-standard cell source for many tissue-engineering therapies and have been successfully applied in clinics [4,5]. However, hBMSCs are hampered by an invasive harvesting procedure, limited availability, and loss of potency in seniors or patients with certain diseases and disorders [6]. Human umbilical cord MSCs (hUCMSCs) are capable of differentiating into mesenchymal lineages. They are easily and abundantly available, with robust proliferation and self-renewal capability due to their origin in neonatal tissues [7]. The main obstacle of hUCMSCs is immunogenic concerns when used heterologously. For autologous applications, the umbilical cord has to be properly cryopreserved from childbirth for an extended period of time.

The breakthrough discovery of induced pluripotent stem cells (iPSCs) by Takahashi et al. and Yu et al. offers the possibility of generating a high yield of custom-tailored stem cells [8,9]. This provides the excitement of turning back somatic cells' developmental clock into pluripotent stem cells. hiPSCs represent an enormous source of patient-specific stem cells derived from easily accessible cells like fibroblasts [10], keratinocytes [11], blood cells [12], etc. Much progress has been achieved in the investigation of iPSCs, from the use of viral integration [8,9] to virus-free or vector-free non-integrating strategies [13,14], and a better understanding of its similarities and differences to embryonic stem cells (ESCs) [15]. With similar pluripotency as ESCs, yet without the ethical or immunogenic concerns related to ESCs, iPSCs are a potentially new frontier for cell-based regenerative medicine [16]. To date, the application of hiPSCs in osteo-regenerative medicine is a relatively new research field. An extensive literature search revealed only 16 papers on the osteogenic differentiation of hiPSCs and potential applications in bone tissue engineering [17-32], including two for periodontal tissue engineering [28,29]. These findings offered evidence that hiPSCs could be induced into mesenchymal or osteoblastic lineages, presenting alkaline phosphatase (ALP) activity, osteogenic gene expression and mineral synthesis. *In vivo* studies demonstrated *de novo* bone formation or mineral deposition in hiPSCs-implanted scaffolds and direct involvement of transplanted cells in bone regeneration [17,20-22,25,27-30]. Thus, hiPSCs or their progeny (hiPSC-derived cells) seeded in appropriate scaffolds could provide a promising strategy for bone tissue engineering.

Calcium phosphate cements have excellent biocompatibility, osteoconductivity, in situ-hardening and molding capabilities and injectability, and can be resorbed and replaced by new bone *in vivo* [33-38]. The first such cement was developed in 1986 and consisted of a mixture of tetracalcium phosphate (TTCP) and dicalcium phosphate anhydrous (DCPA) (referred to as CPC) [39]. CPC was approved in 1996 by the Food and Drug Administration

(FDA) for repairing craniofacial defects. Our previous studies enhanced the mechanical, physical and biological properties of CPC through the introduction of absorbable fibers [40], chitosan [41], mannitol porogen [42], gas-foaming agents [43], alginate microbeads [44], and biofunctionalization [45]. These approaches improved the CPC's mechanical strength, setting time, degradability, macroporosity, cell attachment, and delivery of cells and growth factors. Thus, CPC has great potential for bone repair and augmentation. In the present study, water-soluble mannitol porogens were incorporated into CPC to induce macroporosity [46]. Arg-Gly-Asp (RGD), a short integrin-recognition sequence, was also incorporated into CPC to promote cell attachment to scaffold [45,47]. To date, there has been no report on the comparison of hiPSCs, hUCMSCs and hBMSCs seeded on CPC scaffolds for bone regeneration *in vivo*.

Therefore, the objectives of this study were to: (1) investigate hiPSCs, hUCMSCs and hBMSCs for bone tissue engineering; and (2) seed hiPSCs, hUCMSCs and hBMSCs on biofunctionalized macroporous CPC and compare their bone regeneration efficacy in cranial defects in rats for the first time. The following hypotheses were tested: (1) hiPSCs and hUCMSCs would be viable alternative cell sources for bone tissue engineering, matching the bone regeneration of the gold-standard hBMSCs *in vivo*; (2) all stem cell groups (hiPSCs, hUCMSCs and hBMSCs) would greatly enhance bone regeneration *in vivo*, compared to CPC control without cell seeding; (3) biofunctionalized macroporous CPC would be suitable scaffolds to deliver and support stem cells with a robust bone regeneration capacity.

2. Materials and methods

2.1 Fabrication of RGD-coated macroporous CPC

CPC powder was prepared following previous studies [40-45]. Briefly, TTCP [$Ca_4(PO_4)_2O$] was synthesized using DCPA ($CaHPO_4$) and calcium carbonate (both from J.T. Baker, Philipsburg, NJ) which were mixed and heated at 1500 °C for 6 h in a furnace (Model 51333, Lindberg, Watertown, WI). The heated mixture was quenched to room temperature in a desicator, ground in a ball mill (Retsch PM4, Brinkman, NY) and sieved to obtain TTCP powder with a median particle size of 5 μm. The commercial DCPA powder was ground for 24 h in the ball mill in 95% ethanol and sieved to obtain a median particle size of approximately 1 μm. Then the TTCP and DCPA powders at 1:3 molar ratio were thoroughly mixed in a micromill (Bel-Alert Products, Pequannock, NJ) to form the CPC powder [45,46]. Water-soluble mannitol ($CH_2OH[CHOH]_4CH_2OH$, Sigma, St. Louis, MO) particles were used as a porogen to create macropores in CPC. Mannitol was recrystallized in an ethanol/water solution at 50/50 by volume, dried, ground, and sieved through openings of 500 μm (top sieve) and 300 μm (bottom sieve). The mannitol particles were mixed with CPC powder at a mannitol/(mannitol + CPC powder) mass fraction of 40% [46]. The previous study showed that the CPC paste containing 40% of mannitol was fully injectable under a syringe force of 10 N, and the set CPC scaffold had a macroporosity of (50.9 ± 6.7)% and a total porosity of (82.6 ± 2.4)% by volume [46]. The CPC liquid contained 0.2 M Na_2HPO_4 in distilled water to accelerate the setting reaction [46]. A powder:liquid mass ratio of 2:1 was used to form a flowable CPC paste. The paste was placed in molds with a diameter of 8

mm and a thickness of 1 mm. After incubation in a humidor for 1 d at 37 °C, the disks were demolded and immersed in distilled water at 37 °C for 3 d to dissolve the mannitol. CPC disks were autoclaved, and then placed into 24-well plates with one disk per well. RGD, a well-known integrin recognition sequence, was used to promote cell adhesion on synthetic surfaces [45,47]. Recent studies showed that RGD-biofunctionalized scaffolds exhibited better cell attachment, proliferation, osteogenic differentiation and mineral deposition, than controls [45,47]. Thus, RGD was used in this study to promote cell attachment to CPC. RGD (Sigma) was reconstituted in 0.1 M acetic acid, diluted in phosphate-buffered saline (PBS) to 1000 μg/mL. Each CPC disk was immersed in 100 μL RGD solution for 1 h at 37 °C. When CPC was soaked in the RGD solution, RGD was adsorbed onto the surface and into the pores of the scaffold [48]. In our preliminary study, SEM examination showed that 3 h after cell-seeding, most hiPSC-MSCs on CPC scaffold without RGD were still spherical or fusiform, while cells on CPC scaffold with RGD exhibited a healthy polygonal morphology with spreading cytoplasmic extensions. One day after cell seeding, live/dead staining of hiPSC-MSCs on CPC further confirmed the significant enhancement of cell attachment by soaking CPC scaffold with RGD. Based on the promising preliminary study, the simple method of soaking CPC scaffold in RGD solution was used.

2.2 hiPSCs culture and derivation of hiPSC-MSCs

The culture of hiPSCs was approved by the University of Maryland Institutional Review Board (HP-00046649). Only one cell line per cell type was used in this pilot study. hiPSC BC1 line was derived from adult bone marrow CD34+ cells which were programmed by a single episomal vector pEB-C5 as previously described [49]. Undifferentiated hiPSCs were maintained on mitotically-inactivated murine embryonic fibroblasts (MEF) feeder cells and fed with the hiPSCs culture medium. The hiPSCs culture medium consisted of 80% Dulbecco's modified Eagle medium (DMEM)/F12 (Invitrogen, Carlsbad, CA), 20% Knockout Serum Replacement (a serum-free formulation, Invitrogen), 1% MEM non-essential amino acids solution, 10 ng/mL basic fibroblast growth factor (β-FGF, Invitrogen), 1 mM L-glutamine (Sigma) and 0.1 mM β-mercaptoethanol (Sigma). hiPSCs were detached from a feeder layer and dissociated into clumps through treatment with 1 mg/mL collagenase type IV in DMEM/F12 at 37 °C for 6 min, followed by mechanical scraping. The dissociated hiPSC clumps were collected by sedimentation, resuspended in embryoid body (EB) differentiation medium (the same formulation as hiPSC culture medium but without β-FGF), and transferred to 25 cm^2 ultra-low attachment cell culture flasks (Corning, Corning, NY). After 10 d, the EBs were transferred onto 0.1% gelatin coated culture dishes. Cells growing out from EBs were cultured and upon 70% confluence, the outgrowth cells (P0) were selectively isolated by using cell scrapers and subcultured in MSC growth medium. The MSC growth medium consisted of low glucose Dulbecco's modified Eagle's medium (DMEM, Gibco, Grand Island, NY) supplemented with 10% fetal bovine serum (FBS, HyClone, Logan, UT), 100 U/mL penicillin, and 100 mg/mL streptomycin (PS, Gibco). The differentiated cells from these culture conditions were passaged until a homogeneous fibroblastic morphology appeared. They were termed hiPSC-derived MSCs (referred to as hiPSC-MSCs). Our previous study confirmed that the hiPSC-MSCs generated from this method expressed surface markers characteristic of MSCs (CD29, CD44, CD166,

CD73), and were negative for typical hematopoietic (CD34), endothelial (CD31) and pluripotent markers (TRA-1-81 and OCT 3/4) [23].

2.3 hUCMSCs and hBMSCs culture

hUCMSCs were obtained from ScienCell (Carlsbad, CA), which were harvested from the Wharton's Jelly in umbilical cords of healthy babies. Only one cell line per cell type was used in this pilot study. hUCMSCs were cultured in DMEM with 10% FBS and 1% PS. Immunophenotyping of hUCMSCs were investigated in our previous study via flow cytometry [50]. The hUCMSCs expressed high levels of adhesion markers (CD29 and CD44) and MSC-specific antigen CD105 (also called SH2). The cells were positive for HLA-class I (HLA-ABC), and negative for HLA-Class II (HLA-DR). The cells did not express endothelial marker (CD31) or hematopoietic linage markers (CD34 and CD45). This phenotype is characteristic for MSCs [50].

hBMSCs were obtained from Lonza (Allendale, NJ). hBMSC were maintained in DMEM plus 10% FBS, 1% PS, 0.25% gentamicin and 0.25% fungizone (Invitrogen). Routine characterization of hBMSCs was provided by the manufacture. It included testing for surface antigens and functional testing for differentiation down specific lineage pathways. Cells were tested positive for CD105, CD166, CD29 and CD44, but negative for CD14, CD34, CD45 by flow cytometry.

2.4 Cell attachment and viability

The fifth-passage hiPSC-MSCs, hUCMSCs and hBMSCs were used in the following experiments. Cells were seeded onto the RGD-biofunctionalized CPC disks in 24-well plates at a density of 3×10^5 cells/well [40]. On the second day, the medium was changed into osteogenic medium which consisted of the MSC growth medium supplemented with 100 nM dexamethasone, 10 mM ß-glycerophosphate, 0.05 mM ascorbic acid, and 10 nM 1α,25-dihydroxyvitamin (Sigma) [45].

At 1, 7 and 14 d, live/dead staining (Molecular Probes, Eugene, OR) was used to test cell viability on CPC. Disks were washed with PBS and incubated with 4 mM ethidium homodimer-1 (EthD-1) and 2 mM calcein-AM in PBS for 20 min. The disks were examined using epifluorescence microscopy (Eclipse TE2000-S, Nikon, Melville, NY). The percentage of live cells P and the live cell density D were calculated as previously described [51]. P = number of live cells/(number of live cells + number of dead cells). D = number of live cells in the image/the image area [51]. Two randomly-chosen images for each sample were analyzed with three disks per condition, yielding six images per group at each time point (technical replicates n = 6). The test was independently repeated three times (biological replicates = 3) on three different days by seeding new batches of cells on new batches of CPC disks.

2.5 Osteogenic differentiation and mineralization

For osteogenic differentiation, at 1, 7 and 14 d, RNA was extracted from six cell-seeded disks per group per time point. Two disks were pooled together as an individual RNA sample to have sufficient amount of RNA (technical replicates n = 3). The test was

independently repeated three times (biological replicates = 3) on three different days by seeding new batches of cells on new batches of CPC disks. The total cellular RNA was extracted with TRIzol reagent (Invitrogen) and PureLink RNA Mini Kit (Invitrogen), and then reverse-transcribed into cDNA by a High-capacity cDNA Reverse Transciption kit (Applied Biosystems, Foster City, CA). TaqMan gene expression kits were used to quantify targeted genes on human alkaline phosphatase (ALP, Hs00758162_m1), Runt-related transcription factor (Runx2, Hs00231692_m1), collagen type I (COL1, Hs00164004), osteocalcin (OC, Hs00609452_g1), and glyceraldehyde 3-phosphate dehydrogenase (GAPDH, Hs99999905). Relative expression was evaluated using the $2^{-\Delta\Delta Ct}$ method and normalized by the C_t of the housekeeping gene GAPDH. The C_t value of hiPSC-MSCs, hUCMSCs, hBMSCs cultured on CPC scaffolds in growth medium for 1 d served as the calibrator [51].

For cell mineralization, at 1, 7 and 14 d, disks were fixed with 10% formaldehyde and stained with Alizarin Red S (ARS, Millipore, Billerica, MA) for 1 h. The disks were then rinsed by deionized water four times to visualize the presence of calcified deposition by the cells (technical replicates n = 6) [51]. An Osteogenesis Quantitation Kit (Millipore, ECM 815) was used to extract the stained minerals and measure the ARS concentration, following the manufacturer's instructions (n = 6). Control CPC scaffolds with the same compositions, but without cells, were measured at the same time periods; they were subjected to the same culture medium and incubation conditions as the cell-seeded disks (n = 6). The control's ARS concentration was subtracted from that of the cell-seeded scaffolds to yield the net mineral concentration synthesized by the cells [51]. The test was independently repeated three times (biological replicates = 3).

2.6 In vivo critical-sized cranial defects in rats

Critical-sized cranial defects were created in male athymic nude rats (Hsd:RH-Fox1^{mu}, 8 weeks old, weighing 200-250 g, Harlan, Indianapolis, IN) in accordance with the protocol approved by the University of Maryland (IACUC # 0909014) and NIH guidelines. Under general anesthesia of 75 mg/kg body weight of ketamine and 10 mg/kg of xylazine, a skin incision was made on the midline of cranium. The periosteum was ablated, and a full-thickness standardized trephine defect, 8 mm in diameter, was made in the calvarium under continuous saline buffer irrigation. Cell-seeded CPC scaffolds were maintained in osteogenic media for 14 d before implantation. Cell-free CPC was used as control. Rats were randomly divided into four groups for: hiPSC-MSC-CPC scaffold, hUCMSC-CPC scaffold, hBMSC-CPC scaffold, and CPC control without cells, with six rats per group (technical replicates n = 6). The grafts were harvested at 12 weeks (w) and fixed in 10% formalin.

2.7 Microcomputed tomography (μCT) scanning

Samples harvested at 12 w were scanned with micro-CT (μCT40, Scanco Medical, Bassersdorf, Switzerland). The parameters were set at a resolution of 18 μm, I = 114 μA, E = 70 kVp, with integration time of 300 ms. The image analysis was carried out using the Mimics innovation suite (Version 16.0, Materialise, Plymouth, MI). A three-dimensional region of interest (ROI) was defined as a cylindrical area covering the defect to reconstruct

and analyze each specimen. The function of “Profile Lines” of the Mimics innovation suite was used to evaluate the bone mineral density of the area of focus for each sample. A profile line was drawn from the peripheral host bone, across the defect area to the other side of the defect boundary. The gray values on the profile line were shown in a curve diagram, which were in proportional to the bone mineral density (in a scale from 0 to 255) [52]. The percentage of the increase of bone density in the scaffold comparing to host bone was calculated as: (gray value in scaffold - gray value in host bone)/gray value in host bone (technical replicates n = 6).

2.8 Histomorphometry analyses

Specimens were decalcified and embedded in paraffin. The central region of the implant and defect was cut into 5 μm thick sections and stained with hematoxylin and eosin (H&E) and Masson's Trichrome. The slices were scanned using a Scanscope Digital Slide Scanner (Aperio, Vista, CA) and analyzed by Imagescope software (Aperio). New bone area, new blood vessel number and total defect area were measured within the boundaries of the defect in each H&E section by Image Pro Plus Software (Media Cybernetics, Carlsbad, CA). The perimeter around the new bone was traced, and the area of the new bone was measured by the software. New bone area fraction was calculated as the new bone area divided by the total defect area. Blood vessels were identified by their luminal structure and the presence of red blood cells within their boundaries. New blood vessel density was calculated as the number of new blood vessels in the defect area divided by the entire defect area (technical replicates n = 6) [51].

2.9 Histologic scoring for evaluation of new bone formation

Six samples per group were evaluated and scored with a quantitative grading scale (Table 1) [53,54]. Samples were assessed for: (1) Hard tissue response at the bone-scaffold interface; (2) Bone bridging at the dura side of the defect; and (3) Bone formation within the scaffold pores. Two independent reviewers unaware of treatment groups evaluated all the sections and then reached a consensus on the score for each section. The scores were averaged for each group to determine the overall score for the group (technical replicates n = 6).

2.10 Immunohistochemistry (IHC)

Human origin of engineered bone constructs following *in vivo* implantation was detected using primary antibodies against human nuclei (mouse monoclonal anti-human nuclei; MAB1281). Tissue sections were deparaffinized with xylene, and rehydrated with a graded series of ethanol washes. The epitopes were recovered by incubation in citrate buffer at 70 °C for 40 min, and the endogenous peroxidase activity was blocked with 3% H_2O_2. The slides were then blocked with 1% BSA for 30 min to suppress nonspecific staining and stained with primary antibodies (1:50) overnight in a humidified environment. The specimens were subsequently incubated with secondary antibody against mouse IgG (1:500) for 30 min at 37 °C. Incubation was followed by streptavidin-HRP and diaminobenzidine (DAB) substrate, and counterstaining with hematoxylin solution. Negative controls were performed following the same procedures but without the primary antibody incubation [22].

2.11 Statistical analyses

Statistical analyses were performed using Statistical Package for the Social Sciences (SPSS 17.0, Chicago, IL). All data were expressed as the mean value ± standard deviation (SD). Kolmogorov-Smirn test and Levene test were first performed to confirm the normality and equal variance assumptions of the data were not violated. Statistical significance was analyzed by using one-way analyses of variance (ANOVA), followed by post-hoc LSD (least significant difference) tests. A confidence level of 95% was considered significant.

3. Results

Representative live/dead staining images at 1 d and 14 d are shown in Fig. 1 (A-F). Cells attached and proliferated well on CPC scaffolds. There were numerous live cells (stained green) and a few dead cells (stained red). There were many more cells at 14 d than 1 d due to cell proliferation on CPC. In (G), the percentages of live cells on CPC in all three groups were around 90% and were not significantly different among the three types of cells ($p > 0.1$). In (H), the live cell density on CPC increased with time due to proliferation, with no significant difference among the three types of cells ($p > 0.1$).

Osteogenic differentiation of the three types of stem cells seeded on CPC is plotted in Fig. 2: (A) ALP, (B) Runx2, (C) COL1, and (D) OC gene expressions. The expression of ALP was elevated at 7 d. ALP for hiPSC-MSCs peaked at 7 d, while that for hUCMSCs and hBMSCs peaked at 14 d. Expressions of Runx2 and COL1 peaked at 7 d for all three cell types. OC is an important marker in the late stage of the osteogenic differentiation cascade. The expression of OC in hiPSC-MSCs was down-regulated. In contrast, OC expression was up-regulated for hUCMSCs and hBMSCs.

Representative ARS staining photos of mineral synthesis by hiPSC-MSCs, hUCMSCs and hBMSCs on CPC are shown in Fig. 2 (E). When culture time was increased from 1 to 14 d, the red staining of the synthesized bone mineral matrix became denser and darker, reflecting that mineral synthesis was increased with time in all groups, but without obvious differences among the three types of stem cells. Data from the quantitative osteogenesis assay are plotted in Fig. 2 (F). At each time point, there was no significant difference among the three cell-seeded groups ($p > 0.1$). For each group, the mineral amount synthesized by cells increased dramatically from 1 to 14 days ($p < 0.05$).

Typical sagittal sections of micro-CT scanning obtained from the central area of the defects are shown in Fig. 3. More new bone was found on the dura side in cell-seeded groups than CPC control without cells. The cell-seeded scaffolds exhibited higher signals in comparison to the peripheral host bone (Fig. 3 A, C, D). In CPC control group, no such distinguishable differences were detected (Fig. 3 E). In analyzing the bone mineral density of the scaffold and host bone, a profile line was drawn across the defect area. The bone mineral density was related to the gray values on the profile line. The results reflected an increase of bone density (36.5±11.5)% in cell-seeded scaffolds, and a (6.5 ± 4.9)% increase in CPC control compared to host bone ($p < 0.05$). Overlap of CPC scaffold with new bone deposition contributed to the high density in cell-seeded groups. In contrast, CPC control demonstrated no such effect, suggesting fewer amounts of new bone deposition and mineralization.

Representative histological H&E images are shown in Fig. 4. New bone areas were stained in pink red and marked with arrows. The white areas were due to slight detachment of the tissue or decalcification of CPC. The black and purple areas were residual CPC. The black/dark purple staining of CPC was caused by incomplete decalcification. The outer contour of the cell seeded disks had more new bone and higher calcification than the interior of the scaffold. Two out of six samples in hiPSC-MSC and one of six samples in hUCMSC groups had nearly complete osseous bridge of the defect, where some new bone exhibited an organized and mature bone morphology (Fig. 4A, 4B). Extracellular matrix and new bone deposition filled in the macropores of CPC. CPC control group demonstrated minimal repair with only a limited amount of new bone (Fig. 4D). Cell-seeded groups had significantly more new bone than CPC control group.

Representative Masson's Trichrome staining images of the four groups are shown in Fig. 5. Masson's Trichrome was used to find ossified zones demonstrating the presence of bone tissue in the samples. Fig. 5 shows mineralized (deep blue areas) and nonmineralized osteoid (orange-red) deposited on the dura side and within the pores of the scaffold.

High magnification H&E images of hiPSC-MSCs and hBMSCs seeded scaffolds are shown in Fig. 6 (A, B). Osteocytes and new blood vessels were surrounded by a matrix of woven bone (Fig. 6A). A layer of osteoblasts lined the boundaries of newly formed bone, indicating an active bone regeneration process (Fig. 6B). The macropores were well-formed in shapes of the entrapped mannitol crystals, and were filled with new bone (Fig. 6B).

The new bone area fraction in hiPSC-MSCs constructs (30.4 ± 5.8)% was 2.8-fold that of CPC control (11.0 ± 6.3)% at 12 w ($p < 0.01$) (Fig. 7A). New blood vessels were found residing in new bone. New blood vessel density of hiPSC-MSCs, hUCMSCs and hBMSCs was significant higher than that of CPC control ($p < 0.05$) (Fig. 7B). The histologic scoring for evaluation of new bone formation is shown in Fig. 7C. hiPS-MSC group had the highest score of hard tissue response at bone-scaffold interface ($p < 0.05$), with two out of six samples showing direct bone to implant contact. All the other groups showed fibrous tissue capsules surrounding the implant, but all without inflammatory reactions. Scoring of bone bridging at the dura side showed that the cell-seeded groups far exceeded that of CPC control ($p < 0.05$). For tissue scores inside the pores of CPC, no significant differences were found ($p > 0.1$).

IHC staining for human nuclear antigen is shown in Fig. 8. Positive staining was mainly found within the non-mineralized fibrous tissue in the pores of CPC scaffolds for all cell-seeded groups. These results confirmed the participation of the delivered human cells in the bone regenerative process *in vivo*.

4. Discussion

In this study, we derived MSCs from hiPSCs and compared the performance of hiPSC-MSCs to hUCMSCs and hBMSCs on CPC for bone tissue engineering *in vivo* for the first time. *In vitro* experiments showed that biofunctionized macroporous CPC had good affinity for cell attachment, and no negative effects on cell viability. All three types of cells

underwent osteogenic differentiation. *In vivo* observations revealed neither foreign body reaction nor teratoma formation. New bone deposition and vascularization were found mainly at the dura side and within the macropores of CPC scaffolds. There was no significant difference among three types of stem cells, but there was significantly more new bone in cell-seeded groups than CPC control. Direct participation by the implanted human stem cells in the bone regeneration process in vivo was confirmed by IHC staining.

hiPSCs have the potential to differentiate into cells of all germ layers. However, when transplanted back into patients for specific usage, the hiPSCs need to be induced into high-quality progenitor cells like MSCs, or fully-differentiated homogenous mature cells. Mixed undifferentiated cells are undesirable as they may undergo spontaneous differentiation and give rise to teratomas *in vivo* [55]. There are various protocols to derive MSCs or osteogenic cells from hiPSCs. In this study, we used the same established protocol for differentiating hESCs into MSCs, which involved EB formation [56]. After transferring EBs onto gelatin-coated plates, an outgrowth of epithelial phenotype cells was derived from migration out of EBs, which then underwent epithelial-to-mesenchymal transition (EMT) to acquire the mesenchymal phenotype [57]. Other studies derived MSCs from hiPSCs via simplified protocols without the step of EB formation. Liu et al., reported that by culturing dissociated human pluripotent cells on biomimic, fibrillar, type I collagen coatings, efficient derivation of MSC-like cells from both hESCs and hiPSCs was achieved through this one-step method [24]. Chen et al. derived uniform MSCs from hiPSCs by adding transforming growth factor-β pathway inhibitor SB431542 into the serum-free culture medium of hiPSCs, then culturing in a conventional MSC medium [19]. Another study generated functional MSCs, beginning at a single cell-level, from hiPSCs through a cocktail of growth factor treatment and a combination of fluorescence-activated cell sorting of CD24− and CD105+ [58]. Jin et al., directly induced iPSCs into osteoblastic lineage by culturing iPSCs on poly(caprolactone) scaffolds and adding exogenous osteogenic factors ascorbic acid, beta-glycerophosphate and dexamethasone [21]. Diederichs and Tuan derived MSC-like cells from iPSCs via four different derivation strategies: 1) EB formation, 2) spontaneous differentiation of iPS colonies, 3) mesenchymal co-culture system, and 4) indirect co-culture where iPSCs were seeded on top of cell-free extra cellular matrix from BMSCs and cultured with BMSC-conditioned medium [31]. All four methods succeeded in yielding iPSC-derived MSCs. Their results suggested no significant differences between cells lines via these methods [31]. Furthermore, an *in vivo* skeletal defect microenvironment is also a potent factor which could provide signals to direct differentiation of iPSCs. Levi et al. reported that a hydroxyapatite-coated, bone morphogenetic protein-2(BMP2)-releasing poly-l-lactic acid scaffold combined with a skeletal defect niche was able to guide differentiation of hiPSCs and hESCs for functional integration into new bone regeneration without the need of EB formation or pre-culture under osteogenic supplements [22]. This approach took advantage of the *in vivo* niche in combination of an osteo-inductive scaffold to orchestrate cell fate. Various differentiation protocols all showed that osteogenic differentiation was successfully induced in iPSCs, showing ALP peaks, upregulation of osteogenic-related genes and increased mineral deposition [18-21,23,26-27,30-31].

However, several studies reported that cells derived from hiPSCs did not progress completely to mature osteoblasts *in vitro* due to a lack of expression of late-stage osteogenic makers [24,28], or a relatively lower or delayed expression of osteogenic markers [30,31]. In the present study, osteogenic markers ALP, Runx2, and COL1 were upregulated, while OC was down-regulated in hiPSC-MSCs. Comparing with hUCMSCs and hBMSCs, the results indicated that hiPSC-MSCs were in a less differentiated status under the present induction conditions. This indicates that hiPSC-MSCs likely are less responsive to traditional hBMSC differentiation protocol, and they need more potent osteogenic induction than hUCMSCs and hBMSCs to achieve full commitment to osteogenic lineage.

To enhance the osteogenic differentiation of hiPSCs or hiPSC-derived cells, gene transduction of the cells via potent osteogenic transcription factors is a possible alternative. Recently, Liu et al. transduced BMP2 in hiPSC-MSCs via lentiviral vectors. After 14 d culture in osteogenic medium, ALP activity of BMP2-hiPSC-MSCs was 1.8 times that of untransduced hiPSC-MSCs. When seeded on a RGD-CPC scaffold, COL1A1 and OC expression was 1.9 times and 2.3 times, respectively, that of untransduced cells at 14 d [23]. In addition, it was shown that Runx2 transduction into mouse iPSCs (miPSCs) facilitated the osteogenic differentiation of iPSCs by augmenting the functions of osteoblast markers Runx2, osterix, bone sialoprotein, COL1, OC, ALP activity and bone mineral synthesis [59]. In another study, when miPSCs were transduced with nuclear matrix protein SATB2, the cells yielded elevated ALP activity, up-regulated key osteogenic genes (including late stage markers OC) and increased mineral nodules. Five weeks post-implantation of SATB2-miPSCs with silk scaffolds in a critical-sized calvarial bone defect in nude mice, new bone in SATB2 group was twice that of untransduced cell group and empty vector-transduced cell group [60]. These studies suggested that *ex vivo* gene modification of hiPSCs could effectively enhance the maturation of hiPSC-derived cells before their *in vivo* application.

Despite the lack of late osteogenic marker expression, *in vivo* performance of hiPSC-MSCs in the present study was actually better (albeit slightly) than hUCMSCs and hBMSCs (Fig. 7). This result could be explained from the following four aspects. First, the cranial bone defect provides an osteogenic niche for the transplanted cells [22], which could be potent enough to overwhelm the initial *ex vivo* cell differentiation differences. Second, hiPSC-MSCs were shown to be highly expandable for more than 120 population doublings without obvious senescence, and were still capable to differentiate into multiple cell types [58]. The robust growth potential of hiPSC-MSCs may have contributed to a higher survival rate after transplantation *in vivo* in the present study. Third, *in vitro* osteogenic ability of cells cannot always fully reflect cell performances *in vivo* [61]. In this regard, *in vivo* transplantation test provides the most convincing evidence of the genuine differentiation potential of the stem cells. Literature search revealed only a few *in vivo* studies on hiPSC-derived cells for bone regeneration, for example, in mice/rat critical-sized calvarial bone defects [17,22,25], rat long bone segmental defects [30], mice subcutaneous site [20-21,27,32], and rat periodontal fenestration defect model [29]. These studies concluded that hiPSC-derived cells in conjunction with biomaterials could successfully regenerate new bone. Direct contribution of hiPSCs was identified by positive immunoreactivity to antibodies identifying human origin [20-22,25] or Bromodeoxyuridine (BrdU) labeling [29,32]. The implanted cells were

found in the newly-formed fibrous tissue, embedded within or lining the new bone tissue, and in periodontal ligament like tissue [20-22,25,29,32]. These results indicated functional integration of seeded cells into the regenerated tissue. It was speculated that, initially, the seeded cells directly deposited bone minerals in the scaffold. Then, via cell-mediated paracrine stimulation, the recruited native cells from the host likely took over the responsibility of subsequent bone formation and remodeling [20,22,25,32]. From this fourth aspect, it is possible that the hiPSC-MSCs may be slightly more effective in stimulating and recruiting the host cells to the defect site than the other groups in the present study. Further studies are needed to investigate these aspects.

In the present study, new bone was mainly found on the dura side, where cell-seeded side was in contact to dura. This can be attributed to better vascularization on the dura side. Furthermore, comparing cell-seeded groups with CPC control, it was evident that the seeded cells were involved in bone formation, consistent with a previous report [51]. There was also a considerable amount of extra cellular matrix deposition, osteoid and new bone formation within the pores of CPC scaffolds. According to a previous study, CPC without mannitol had only micropores ranging from about 1 to 20 μm [46]. The macropores, generated after dissolution of mannitol, were well-formed in shapes of entrapped mannitol crystals, with a width of 100-400 μm and a length of 200-600 μm [46]. The total pore volume fraction in CPC was approximately 82.6%, while the macropore volume fraction was about 50.9% [46]. Pore sizes of at least 100 μm were needed for bone ingrowth, and pore sizes ranging from 300-400 μm were most favorable for new bone formation [62]. Therefore, in the present study, the interconnected pores formed by mannitol dissolution in CPC likely facilitated the diffusion of oxygen and nutrients, cell migration and proliferation, vascularization, and finally led to new bone formation within the porous structures.

The lack of sufficient vascularization is the major hindrance in creation of functional and viable tissue implants [63]. Promoting angiogenesis of tissue-engineered bone can advance cell performance and promote bone regeneration [64,65]. In the present study, not only was the tubular structure formed by dissolved mannitol beneficial for vascularization, but the seeded cells also made contributions. Proangiogenic actions of hBMSCs, hUCMSCs and hiPSCs were shown in various ischmia conditions [58,66-70]. This favorable effect appeared to derive from the enhanced neovascularization by MSC-mediated angiogenic factors, such as vascular endothelial growth factor (VEGF), to recruit endothelial cells (ECs) [66-68], and by transdifferentiating into endothelial cells [69,70]. In a comparison of the therapeutic effects of hiPSC-MSCs and hBMSCs to treat limb ischemia in mice, hiPSC-MSCs achieved a better result than hBMSCs [58]. This may be attributable to higher survival rate of hiPSC-MSCs after transplantation than hBMSCs [58]. In the present study, hiPSC-MSCs, hUCMSCs and hBMSCs all showed beneficial effects to elicit angiogenic activity, compared to CPC control. Furthermore, the recruited endogenous ECs could further modulate osteogenesis by producing BMPs [71]. The intricate interactions between osteogenesis and angiogenesis likely played a critical role in bone regeneration.

Still, several challenges must be solved for clinical applications of hiPSCs. First, researchers are looking for an efficient, safe and reliable way to trigger the reprogramming process. Non-integration methods will gradually replace genomic integrative vectors [72]. Second, it

is reported that epigenetic memory from the original cell source may favor differentiation of some iPSCs down specific pathways [73]. An important next step will be to identify the best starting somatic cells for iPSCs that can be sufficiently osteogenically-inducted for the replenishment of osteoblasts to recover structures and functions of bone. The third challenge is to achieve complete commitment of iPSCs to the osteoblastic lineage. Optimization of the induction protocols to obtain a pure population of induced target cells is needed, in order to reduce or even eliminate the risk of teratoma formation and guarantee bone regeneration efficiency [74].

The present study has several limitations. First, there was only one cell line per cell type tested. Considering the high degree of donor-dependent variability of MSCs and the complexity of hiPSCs, a further study should include the testing of several different cell lines for each cell type and how they may differ in bone regeneration. Second, an empty defect (blank control) was not included as a control in the present study, based on literature that the 8 mm cranial defect in rats is generally accepted as a critical sized defect. It would be interesting to examine the new bone formation differences in blank control, CPC scaffold control, and CPC scaffold seeded with various types of stem cells.

5. Conclusions

The present study showed for the first time that hiPSCs had comparable *in vivo* bone regeneration and angiogenic capability to hBMSCs and hUCMSCs in critical-sized cranial defects in rats. The hiPSC-MSC-CPC constructs generated new bone that was 2.8-fold that of CPC control without cell seeding. Therefore, hiPSCs and hUCMSCs may represent viable alternatives to hBMSCs, which require an invasive procedure to harvest yielding only limited amount of cells. Biofunctionalized macroporous CPC scaffold appeared to be suitable for delivering hiPSC-MSCs, hUCMSCs and hBMSCs for bone tissue engineering. The stem cell-CPC constructs displayed a robust capacity for bone regeneration and are promising for bone regeneration in dental, craniofacial and orthopedic applications.

Acknowledgements

We thank Drs. Carl G. Simon, Laurence C. Chow, and David J. Mooney for discussions. We thank Dr. Linzhao Cheng for generously providing the hiPSC BC1 cell line. This study was supported by NIH R01 DE14190 and R21 DE22625 (HX), National Science Foundation of China 81401794 (PW), 31100695 and 31328008 (LZ), U01 DE023752 (JS for μCT), Maryland Stem Cell Research Fund (HX), and University of Maryland School of Dentistry.

References

1. Amini AR, Laurencin CT, Nukavarapu SP. Bone tissue engineering: recent advances and challenges. Crit Rev Biomed Eng. 2012; 40:363–408. [PubMed: 23339648]
2. O'Keefe RJ, Mao J. Bone tissue engineering and regeneration: from discovery to the clinic--an overview. Tissue Eng Part B Rev. 2011; 17:389–92. [PubMed: 21902614]
3. Ducheyne P, Mauck RL, Smith DH. Biomaterials in the repair of sports injuries. Nat Mater. 2012; 11:652–4. [PubMed: 22825010]
4. Steinert AF, Rackwitz L, Gilbert F, Noth U, Tuan RS. Concise review: the clinical application of mesenchymal stem cells for musculoskeletal regeneration: current status and perspectives. Stem Cells Transl Med. 2012; 1:237–47. [PubMed: 23197783]

5. Charbord P. Bone marrow mesenchymal stem cells: historical overview and concepts. Hum Gene Ther. 2010; 21:1045–56. [PubMed: 20565251]
6. Bianco P, Robey PG, Saggio I, Riminucci M. “Mesenchymal” stem cells in human bone marrow (skeletal stem cells): a critical discussion of their nature, identity, and significance in incurable skeletal disease. Hum Gene Ther. 2010; 21:1057–66. [PubMed: 20649485]
7. Lee OK, Kuo TK, Chen WM, Lee KD, Hsieh SL, Chen TH. Isolation of multipotent mesenchymal stem cells from umbilical cord blood. Blood. 2004; 103:1669–75. [PubMed: 14576065]
8. Takahashi K, Yamanaka S. Induction of pluripotent stem cells from mouse embryonic and adult fibroblast cultures by defined factors. Cell. 2006; 126:663–76. [PubMed: 16904174]
9. Yu J, Vodyanik MA, Smuga-Otto K, Antosiewicz-Bourget J, Frane JL, Tian S, et al. Induced pluripotent stem cell lines derived from human somatic cells. Science. 2007; 318:1917–20. [PubMed: 18029452]
10. Park IH, Zhao R, West JA, Yabuuchi A, Huo H, Ince TA, et al. Reprogramming of human somatic cells to pluripotency with defined factors. Nature. 2008; 451:141–6. [PubMed: 18157115]
11. Li W, Zhou H, Abujarour R, Zhu S, Young Joo J, Lin T, et al. Generation of human-induced pluripotent stem cells in the absence of exogenous Sox2. Stem Cells. 2009; 27:2992–3000. [PubMed: 19839055]
12. Loh YH, Agarwal S, Park IH, Urbach A, Huo H, Heffner GC, et al. Generation of induced pluripotent stem cells from human blood. Blood. 2009; 113:5476–9. [PubMed: 19299331]
13. Kim D, Kim CH, Moon JI, Chung YG, Chang MY, Han BS, et al. Generation of human induced pluripotent stem cells by direct delivery of reprogramming proteins. Cell Stem Cell. 2009; 4:472–6. [PubMed: 19481515]
14. Warren L, Manos PD, Ahfeldt T, Loh YH, Li H, Lau F, et al. Highly efficient reprogramming to pluripotency and directed differentiation of human cells with synthetic modified mRNA. Cell Stem Cell. 2010; 7:618–30. [PubMed: 20888316]
15. Amabile G, Meissner A. Induced pluripotent stem cells: current progress and potential for regenerative medicine. Trends Mol Med. 2009; 15:59–68. [PubMed: 19162546]
16. Vogel G. Breakthrough of the year. Reprogramming cells. Science. 2008; 322:1766–7. [PubMed: 19095902]
17. Ardeshirylajimi A, Dinarvand P, Seyedjafari E, Langroudi L, Jamshidi Adegani F, Soleimani M. Enhanced reconstruction of rat calvarial defects achieved by plasma-treated electrospun scaffolds and induced pluripotent stem cells. Cell Tissue Res. 2013; 354:849–60. [PubMed: 23955642]
18. Ardeshirylajimi A, Hosseinkhani S, Parivar K, Yaghmaie P, Soleimani M. Nanofiber-based polyethersulfone scaffold and efficient differentiation of human induced pluripotent stem cells into osteoblastic lineage. Mol Biol Rep. 2013; 40:4287–94. [PubMed: 23657591]
19. Chen YS, Pelekanos RA, Ellis RL, Horne R, Wolvetang EJ, Fisk NM. Small molecule mesengenic induction of human induced pluripotent stem cells to generate mesenchymal stem/stromal cells. Stem Cells Transl Med. 2012; 1:83–95. [PubMed: 23197756]
20. de Peppo GM, Marcos-Campos I, Kahler DJ, Alsalman D, Shang L, Vunjak-Novakovic G, et al. Engineering bone tissue substitutes from human induced pluripotent stem cells. Proc Natl Acad Sci USA. 2013; 110:8680–5. [PubMed: 23653480]
21. Jin GZ, Kim TH, Kim JH, Won JE, Yoo SY, Choi SJ, et al. Bone tissue engineering of induced pluripotent stem cells cultured with macrochanneled polymer scaffold. J Biomed Mater Res Part A. 2013; 101:1283–91.
22. Levi B, Hyun JS, Montoro DT, Lo DD, Chan CK, Hu S, et al. In vivo directed differentiation of pluripotent stem cells for skeletal regeneration. Proc Natl Acad Sci USA. 2012; 109:20379–84. [PubMed: 23169671]
23. Liu J, Chen W, Zhao Z, Xu HH. Reprogramming of mesenchymal stem cells derived from iPSCs seeded on biofunctionalized calcium phosphate scaffold for bone engineering. Biomaterials. 2013; 34:7862–72. [PubMed: 23891395]
24. Liu Y, Goldberg AJ, Dennis JE, Gronowicz GA, Kuhn LT. One-step derivation of mesenchymal stem cell (MSC)-like cells from human pluripotent stem cells on a fibrillar collagen coating. PLoS One. 2012; 7:e33225. [PubMed: 22457746]

25. Villa-Diaz LG, Brown SE, Liu Y, Ross AM, Lahann J, Parent JM, et al. Derivation of mesenchymal stem cells from human induced pluripotent stem cells cultured on synthetic substrates. Stem Cells. 2012; 30:1174–81. [PubMed: 22415987]
26. Tang M, Chen W, Liu J, Weir MD, Cheng L, Xu HH. Human induced pluripotent stem cell-derived mesenchymal stem cell seeding on calcium phosphate scaffold for bone regeneration. Tissue Eng Part A. 2014; 20:1295–305. [PubMed: 24279868]
27. Zou L, Luo Y, Chen M, Wang G, Ding M, Petersen CC, et al. A simple method for deriving functional MSCs and applied for osteogenesis in 3D scaffolds. Sci Rep. 2013; 3:2243. [PubMed: 23873182]
28. Duan X, Tu Q, Zhang J, Ye J, Sommer C, Mostoslavsky G, et al. Application of induced pluripotent stem (iPS) cells in periodontal tissue regeneration. J Cell Physiol. 2011; 226:150–7. [PubMed: 20658533]
29. Hynes K, Menicanin D, Han J, Marino V, Mrozik K, Gronthos S, et al. Mesenchymal stem cells from iPS cells facilitate periodontal regeneration. J Dent Res. 2013; 92:833–9. [PubMed: 23884555]
30. Ko JY, Park S, Im GI. Osteogenesis from human induced pluripotent stem cells: an in vitro and in vivo comparison with mesenchymal stem cells. Stem Cells Dev. 2014
31. Diederichs S, Tuan RS. Functional comparison of human-induced pluripotent stem cell-derived mesenchymal cells and bone marrow-derived mesenchymal stromal cells from the same donor. Stem Cells Dev. 2014
32. Hynes K, Menicanin D, Mrozik K, Gronthos S, Bartold PM. Generation of functional mesenchymal stem cells from different induced pluripotent stem cell lines. Stem Cells Dev. 2014; 23:1084–96. [PubMed: 24367908]
33. Chow LC. Next generation calcium phosphate-based biomaterials. Dent Mater J. 2009; 28:1–10. [PubMed: 19280963]
34. Bohner M. Design of ceramic-based cements and putties for bone graft substitution. Eur Cell Mater. 2010; 20:1–12. [PubMed: 20574942]
35. Ginebra MP, Espanol M, Montufar EB, Perez RA, Mestres G. New processing approaches in calcium phosphate cements and their applications in regenerative medicine. Acta Biomater. 2010; 6:2863–73. [PubMed: 20123046]
36. Sariibrahimoglu K, Wolke JG, Leeuwenburgh SC, Yubao L, Jansen JA. Injectable biphasic calcium phosphate cements as a potential bone substitute. J Biomed Mater Res B Appl Biomater. 2014; 102:415–22. [PubMed: 24106108]
37. Grover LM, Wright AJ, Gbureck U, Bolarinwa A, Song J, Liu Y, et al. The effect of amorphous pyrophosphate on calcium phosphate cement resorption and bone generation. Biomaterials. 2013; 34:6631–7. [PubMed: 23747007]
38. Zhang J, Liu W, Schnitzler V, Tancret F, Bouler JM. Calcium phosphate cements for bone substitution: chemistry, handling and mechanical properties. Acta Biomater. 2014; 10:1035–49. [PubMed: 24231047]
39. Brown, WE.; Chow, LC. A new calcium phosphate water setting cement.. In: Brown, PW., editor. Cements research progress. American Ceramics Society; Westerville, OH: 1986. p. 352-79.
40. Zhou H, Weir MD, Xu HH. Effect of cell seeding density on proliferation and osteodifferentiation of umbilical cord stem cells on calcium phosphate cement-fiber scaffold. Tissue Eng Part A. 2011; 17:2603–13. [PubMed: 21745111]
41. Weir MD, Xu HH. Osteoblastic induction on calcium phosphate cement-chitosan constructs for bone tissue engineering. J Biomed Mater Res A. 2010; 94:223–33. [PubMed: 20166217]
42. Tang M, Weir MD, Xu HH. Mannitol-containing macroporous calcium phosphate cement encapsulating human umbilical cord stem cells. J Tissue Eng Regen Med. 2012; 6:214–24. [PubMed: 21442765]
43. Chen W, Zhou H, Tang M, Weir MD, Bao C, Xu HH. Gas-foaming calcium phosphate cement scaffold encapsulating human umbilical cord stem cells. Tissue Eng Part A. 2012; 18:816–27. [PubMed: 22011243]
44. Weir MD, Xu HH. Human bone marrow stem cell-encapsulating calcium phosphate scaffolds for bone repair. Acta Biomater. 2010; 6:4118–26. [PubMed: 20451676]

45. Thein-Han W, Liu J, Xu HH. Calcium phosphate cement with biofunctional agents and stem cell seeding for dental and craniofacial bone repair. Dent Mater. 2012; 28:1059–70. [PubMed: 22809583]
46. Xu HH, Weir MD, Burguera EF, Fraser AM. Injectable and macroporous calcium phosphate cement scaffold. Biomaterials. 2006; 27:4279–87. [PubMed: 16650891]
47. Morgan AW, Roskov KE, Lin-Gibson S, Kaplan DL, Becker ML, Simon CG Jr. Characterization and optimization of RGD-containing silk blends to support osteoblastic differentiation. Biomaterials. 2008; 29:2556–63. [PubMed: 18325585]
48. Biswas S, Becker U. Molecular Modeling of Cell Adhesion Peptides on Hydroxyapatite and TiO2 surfaces: implication in biomedical implant devices. J Biomater Nanobiotechnol. 2013; 4:351–56.
49. Chou BK, Mali P, Huang X, Ye Z, Dowey SN, Resar LM, et al. Efficient human iPS cell derivation by a non-integrating plasmid from blood cells with unique epigenetic and gene expression signatures. Cell Res. 2011; 21:518–29. [PubMed: 21243013]
50. Thein-Han W, Xu HH. Collagen-calcium phosphate cement scaffolds seeded with umbilical cord stem cells for bone tissue engineering. Tissue engineering Part A. 2011; 17:2943–54. [PubMed: 21851269]
51. Chen W, Liu J, Manuchehrabadi N, Weir MD, Zhu Z, Xu HH. Umbilical cord and bone marrow mesenchymal stem cell seeding on macroporous calcium phosphate for bone regeneration in rat cranial defects. Biomaterials. 2013; 34:9917–25. [PubMed: 24054499]
52. Cheng YL, Lin YT, Shih KS. Rapid Prototyping Mandible Model for Dental Implant Surgery Simulation. Comput Aided Des Appl. 2012; 9:177–85.
53. Ohgushi H, Goldberg VM, Caplan AI. Repair of bone defects with marrow cells and porous ceramic. Experiments in rats. Acta orthop Scand. 1989; 60:334–9. [PubMed: 2665415]
54. Patel ZS, Young S, Tabata Y, Jansen JA, Wong ME, Mikos AG. Dual delivery of an angiogenic and an osteogenic growth factor for bone regeneration in a critical size defect model. Bone. 2008; 43:931–40. [PubMed: 18675385]
55. Hayashi T, Misawa H, Nakahara H, Noguchi H, Yoshida A, Kobayashi N, et al. Transplantation of osteogenically differentiated mouse iPS cells for bone repair. Cell Transplant. 2012; 21:591–600. [PubMed: 22793068]
56. Brown SE, Tong W, Krebsbach PH. The derivation of mesenchymal stem cells from human embryonic stem cells. Cells Tissues Organs. 2009; 189:256–60. [PubMed: 18728355]
57. Boyd NL, Robbins KR, Dhara SK, West FD, Stice SL. Human embryonic stem cell-derived mesoderm-like epithelium transitions to mesenchymal progenitor cells. Tissue Eng Part A. 2009; 15:1897–907. [PubMed: 19196144]
58. Lian Q, Zhang Y, Zhang J, Zhang HK, Wu X, Lam FF, et al. Functional mesenchymal stem cells derived from human induced pluripotent stem cells attenuate limb ischemia in mice. Circulation. 2010; 121:1113–23. [PubMed: 20176987]
59. Tashiro K, Inamura M, Kawabata K, Sakurai F, Yamanishi K, Hayakawa T, et al. Efficient adipocyte and osteoblast differentiation from mouse induced pluripotent stem cells by adenoviral transduction. Stem Cells. 2009; 27:1802–11. [PubMed: 19544436]
60. Ye JH, Xu YJ, Gao J, Yan SG, Zhao J, Tu Q, et al. Critical-size calvarial bone defects healing in a mouse model with silk scaffolds and SATB2-modified iPSCs. Biomaterials. 2011; 32:5065–76. [PubMed: 21492931]
61. Kuznetsov SA, Cherman N, Robey PG. In vivo bone formation by progeny of human embryonic stem cells. Stem Cells Dev. 2011; 20:269–87. [PubMed: 20590404]
62. Tsuruga E, Takita H, Itoh H, Wakisaka Y, Kuboki Y. Pore size of porous hydroxyapatite as the cell-substratum controls BMP-induced osteogenesis. J Biochem. 1997; 121:317–24. [PubMed: 9089406]
63. Johnson PC, Mikos AG, Fisher JP, Jansen JA. Strategic directions in tissue engineering. Tissue Eng. 2007; 13:2827–37. [PubMed: 18052823]
64. Patel ZS, Mikos AG. Angiogenesis with biomaterial-based drug- and cell-delivery systems. Journal of biomaterials science Polymer edition. 2004; 15:701–26. [PubMed: 15255521]
65. Lovett M, Lee K, Edwards A, Kaplan DL. Vascularization strategies for tissue engineering. Tissue engineering Part B Reviews. 2009; 15:353–70. [PubMed: 19496677]

66. Al-Khaldi A, Al-Sabti H, Galipeau J, Lachapelle K. Therapeutic angiogenesis using autologous bone marrow stromal cells: improved blood flow in a chronic limb ischemia model. Ann Thorac Surg. 2003; 75:204–9. [PubMed: 12537217]

67. Sato T, Iso Y, Uyama T, Kawachi K, Wakabayashi K, Omori Y, et al. Coronary vein infusion of multipotent stromal cells from bone marrow preserves cardiac function in swine ischemic cardiomyopathy via enhanced neovascularization. Lab Invest. 2011; 91:553–64. [PubMed: 21283079]

68. Edwards SS, Zavala G, Prieto CP, Elliott M, Martinez S, Egana JT, et al. Functional analysis reveals angiogenic potential of human mesenchymal stem cells from Wharton's jelly in dermal regeneration. Angiogenesis. 2014

69. Samuel R, Daheron L, Liao S, Vardam T, Kamoun WS, Batista A, et al. Generation of functionally competent and durable engineered blood vessels from human induced pluripotent stem cells. Proc Natl Acad Sci USA. 2013; 110:12774–9. [PubMed: 23861493]

70. Silva GV, Litovsky S, Assad JA, Sousa AL, Martin BJ, Vela D, et al. Mesenchymal stem cells differentiate into an endothelial phenotype, enhance vascular density, and improve heart function in a canine chronic ischemia model. Circulation. 2005; 111:150–6. [PubMed: 15642764]

71. Kaigler D, Krebsbach PH, West ER, Horger K, Huang YC, Mooney DJ. Endothelial cell modulation of bone marrow stromal cell osteogenic potential. FASEB J. 2005; 19:665–7. [PubMed: 15677693]

72. Robinton DA, Daley GQ. The promise of induced pluripotent stem cells in research and therapy. Nature. 2012; 481:295–305. [PubMed: 22258608]

73. Polo JM, Liu S, Figueroa ME, Kulalert W, Eminli S, Tan KY, et al. Cell type $_{of}$ origin influences the molecular and functional properties of mouse induced pluripotent stem cells. Nat Biotechnol. 2010; 28:848–55. [PubMed: 20644536]

74. Jung Y, Bauer G, Nolta JA. Concise review: Induced pluripotent stem cell-derived mesenchymal stem cells: progress toward safe clinical products. Stem Cells. 2012; 30:42–7. [PubMed: 21898694]

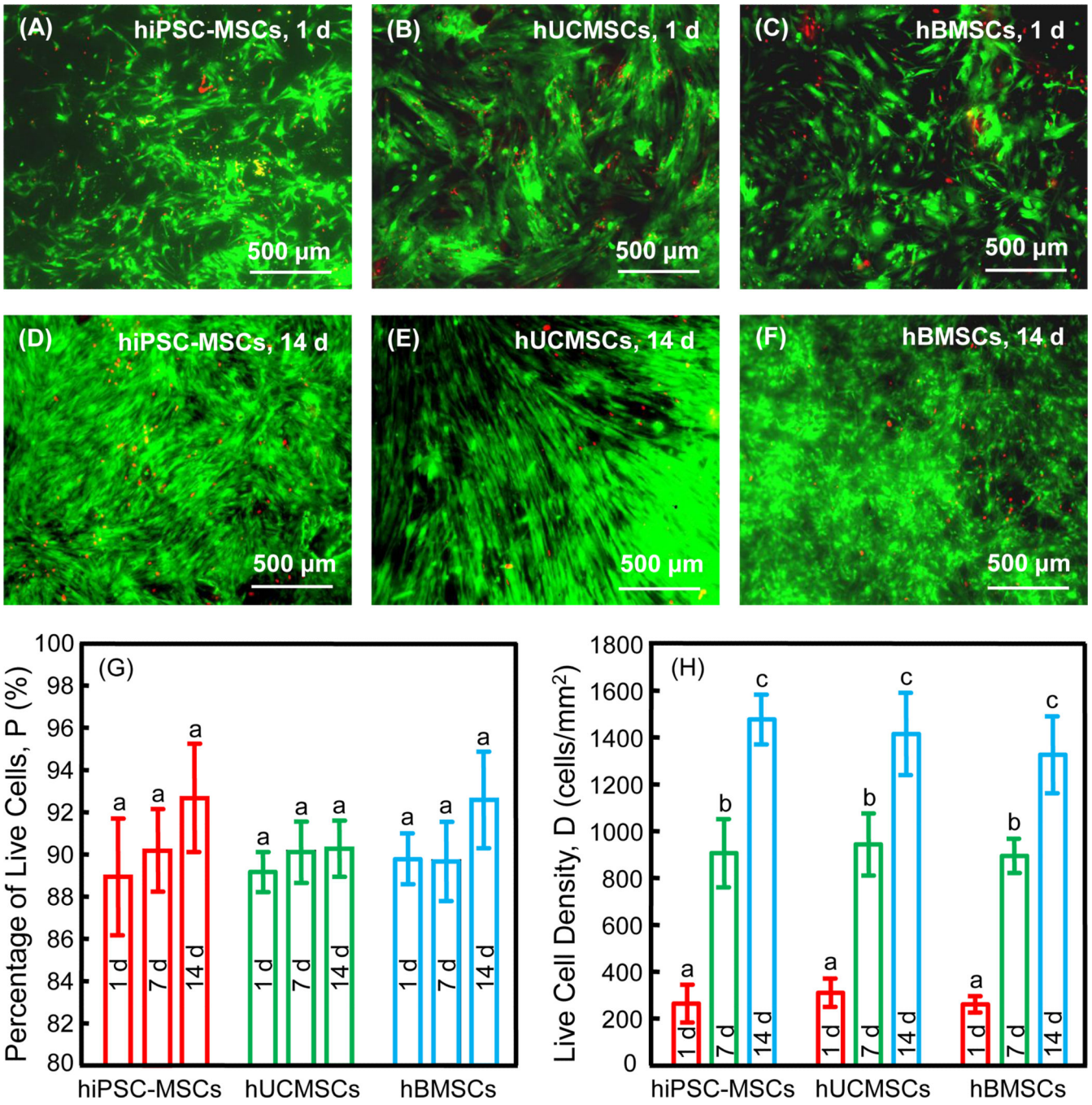

Figure 1.

Cell viability when seeded on CPC scaffold. Live/dead staining of cells at 1d and 14 d are shown in A-F. In all three groups, live cells were abundant, and dead cells were few. Percentage of live cells on CPC was around 90% (G). All groups exhibited increasing live cell density (H). Bars with dissimilar letters indicate significantly different values ($p < 0.05$). Each value is mean ± sd (technical replicates n = 6). The test was independently repeated three times (biological replicates = 3).

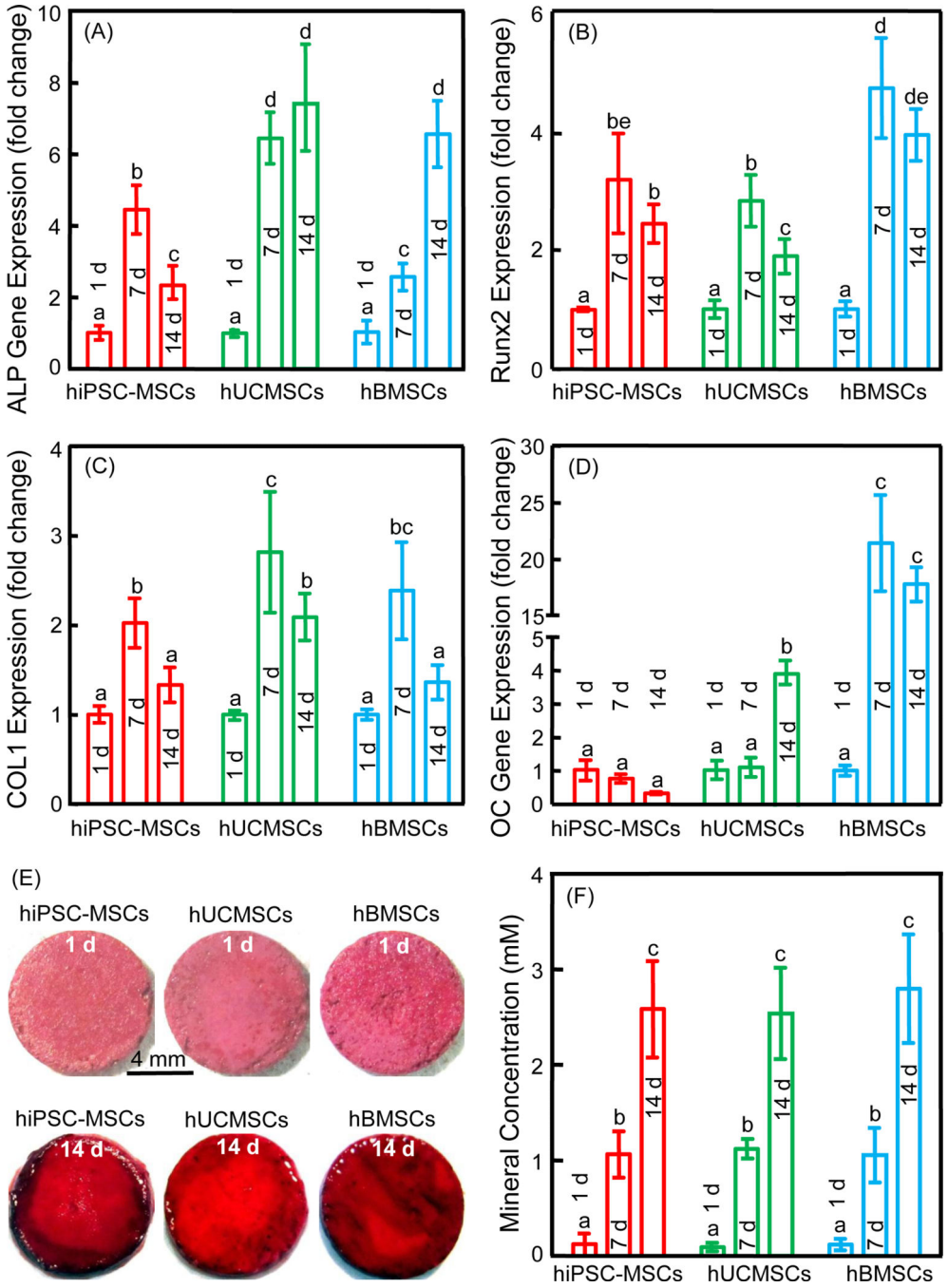

Figure 2.

Osteogenic differentiation of cells on CPC. RT-PCR results for ALP (A), Runx2 (B), COL1 (C), and OC (D). Each value is mean ± sd (technical replicates n = 3). The test was independently repeated three times (biological replicates = 3). Osteogenic markers were upregulated in all groups. OC, the late osteogenic marker, decreased in hiPSC-MSCs group, indicating that hiPSC-MSCs did not progress completely to mature osteoblasts in the *in vitro* induction. Mineral synthesis by cells was detected by Alizarin Red staining (E). The bone mineral matrix became denser and darker red with increasing time. Cell-synthesized mineral

concentration was measured by the osteogenesis assay (F) (technical replicates n = 6 for mineralization). The test was independently repeated three times (biological replicates = 3). Bars with dissimilar letters indicate significantly different values ($p < 0.05$).

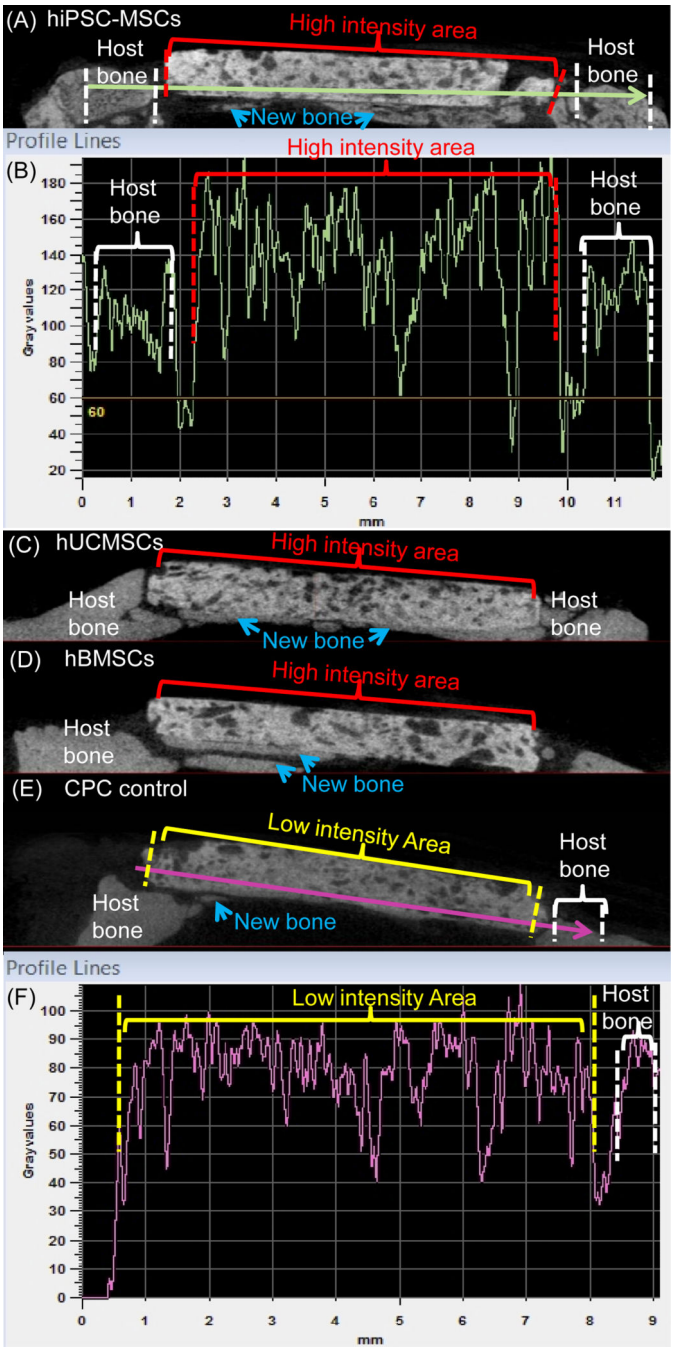

Figure 3.

Representative sagital micro-CT images of hiPSC-MSC-CPC (A), hUCMSCs (C), hBMSCs (D), and CPC control (E). Profile lines are shown for hiPSC-MSC-CPC (B), and CPC control (F). New bone is marked by arrows. A profile line was draw from the peripheral host bone, across the defect area to the other side of the defect boundary. The gray values on profile line were demonstrated in a curve diagram. Cell-seeded scaffolds exhibited higher signals (high intensity areas) than peripheral host bone. In contrast, CPC control had no such distinguishable differences in bone density, indicating less new bone.

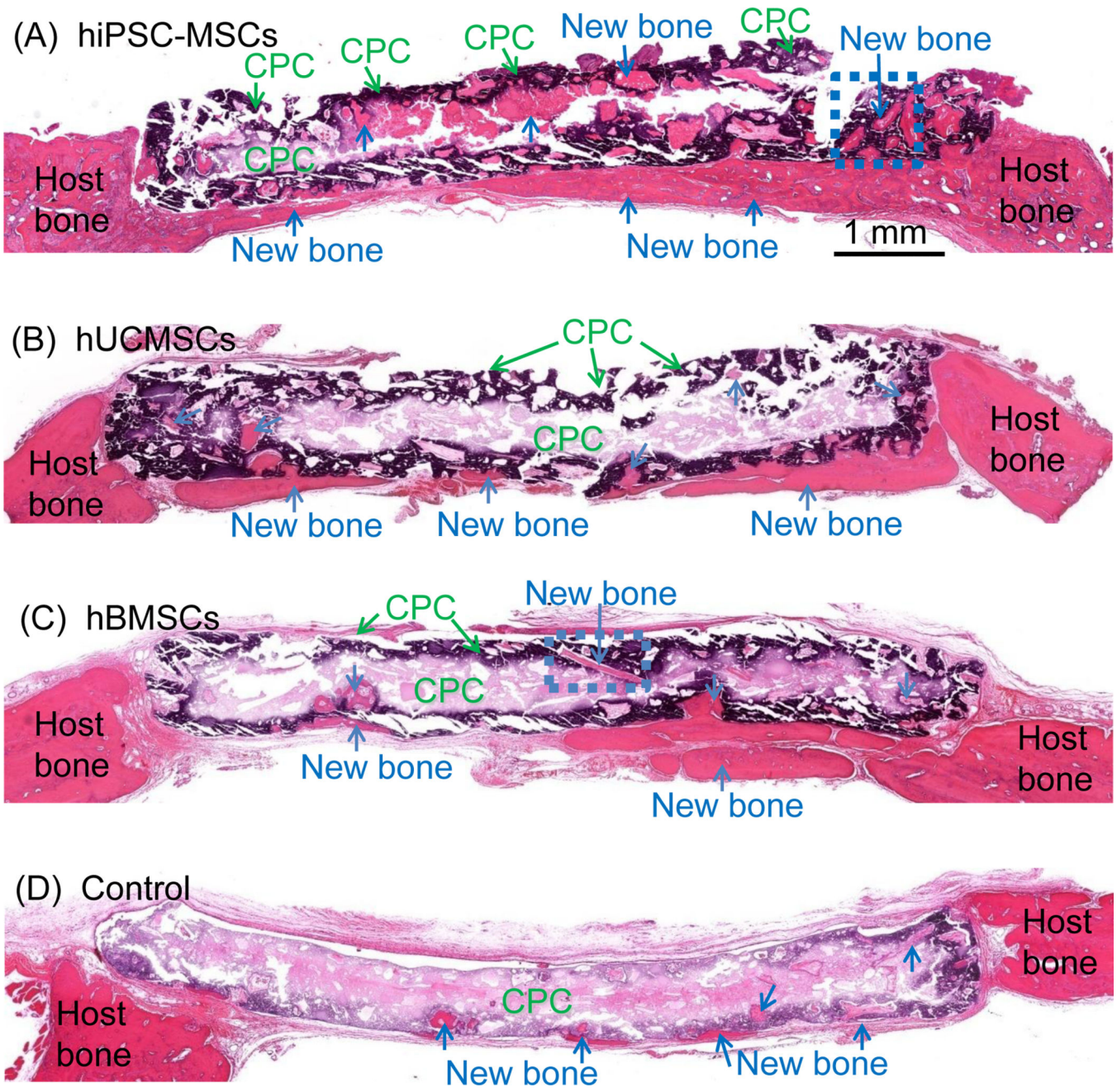

Figure 4.

Representative H&E images. New bone areas were stained in pink red (arrows). The white area was due to slight detachment of the tissue or decalcification of CPC. The dark, dark purple and light purple areas were residual CPC. The periosteal side is on the top side, while the dura side is at the bottom. New bone (arrows) was mainly found on the dura side, and some new bone was deposited within the macropores of CPC. There was more new bone in cell-seeded groups than cell-free control.

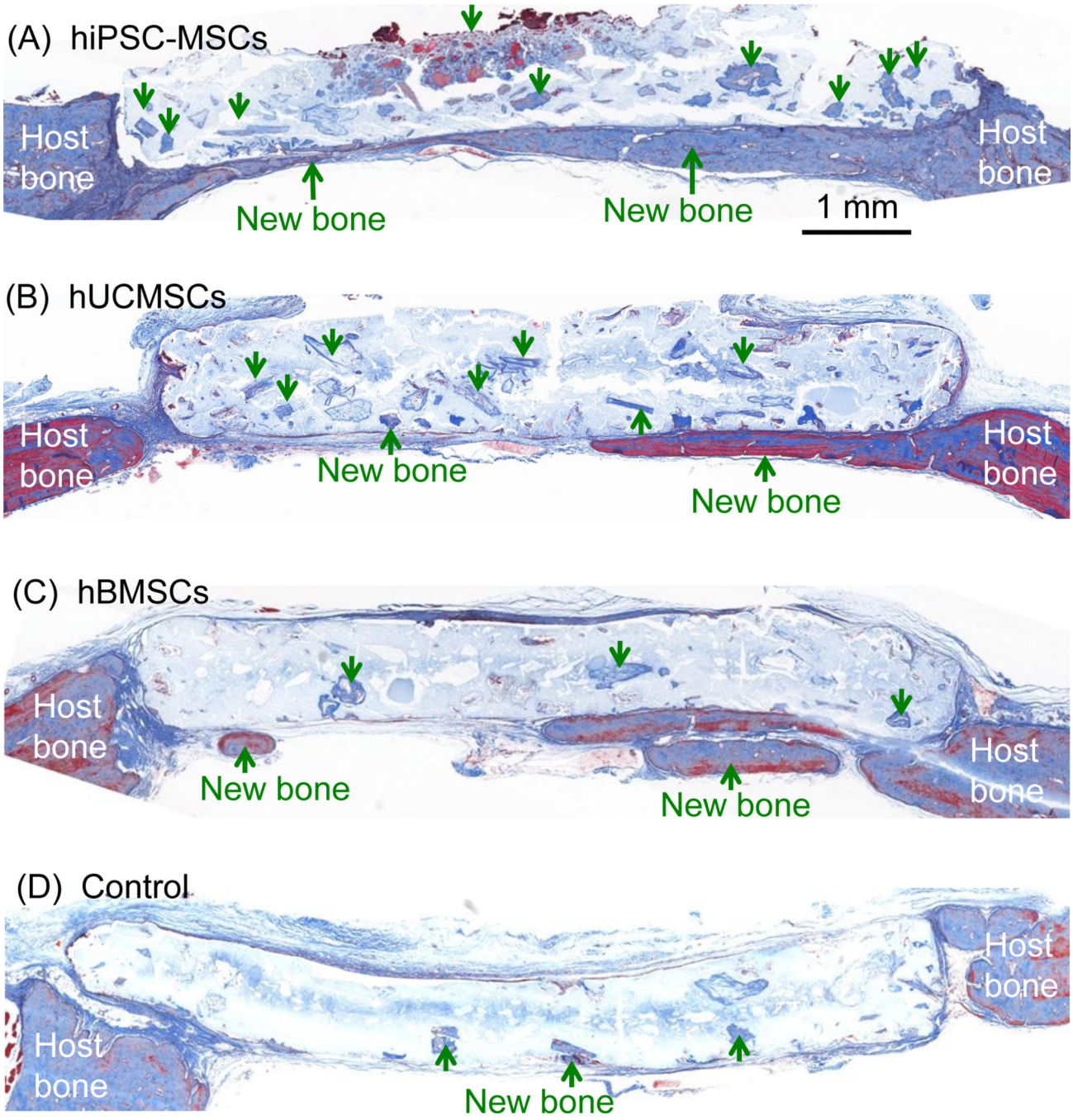

Figure 5.

Representative Masson's Trichrome staining images. In cell-seeded groups, mineralized (deep blue areas) and nonmineralized osteoid (orange-red) mainly deposited on the dura side, and some new bone was formed within the pores of the scaffold. CPC control group had much less new bone.

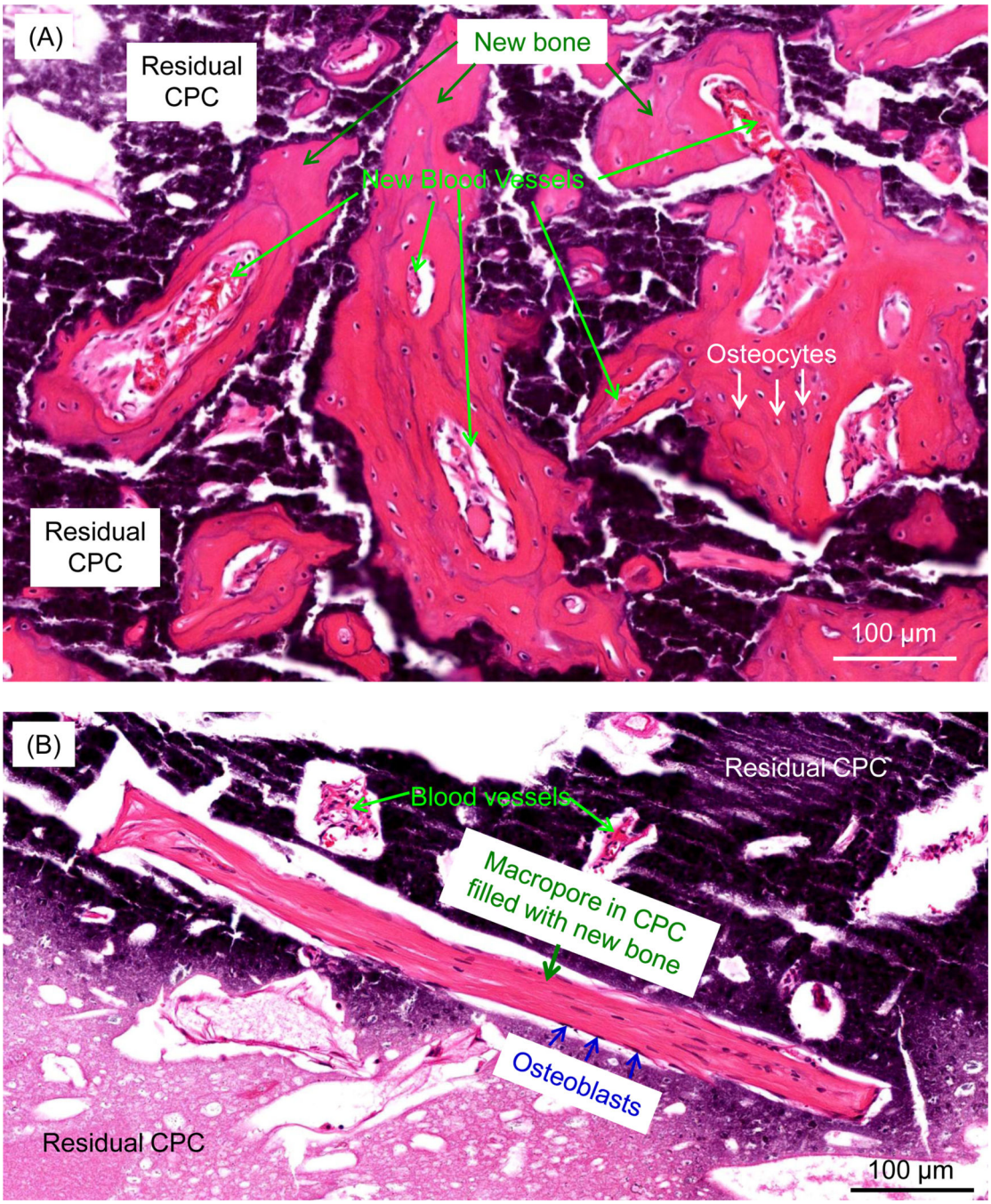

Figure 6.

High magnification images of new bone within the dotted rectangles in Fig. 4A and C, respectively. (A) hiPSC-MSCs, (B) hBMSCs. Macropores from mannitol dissolution were filled with new bone. Osteoblasts lined on the surface of new bone. Osteocytes resided in the bone lacuna. New blood vessels were present in the new bone area.

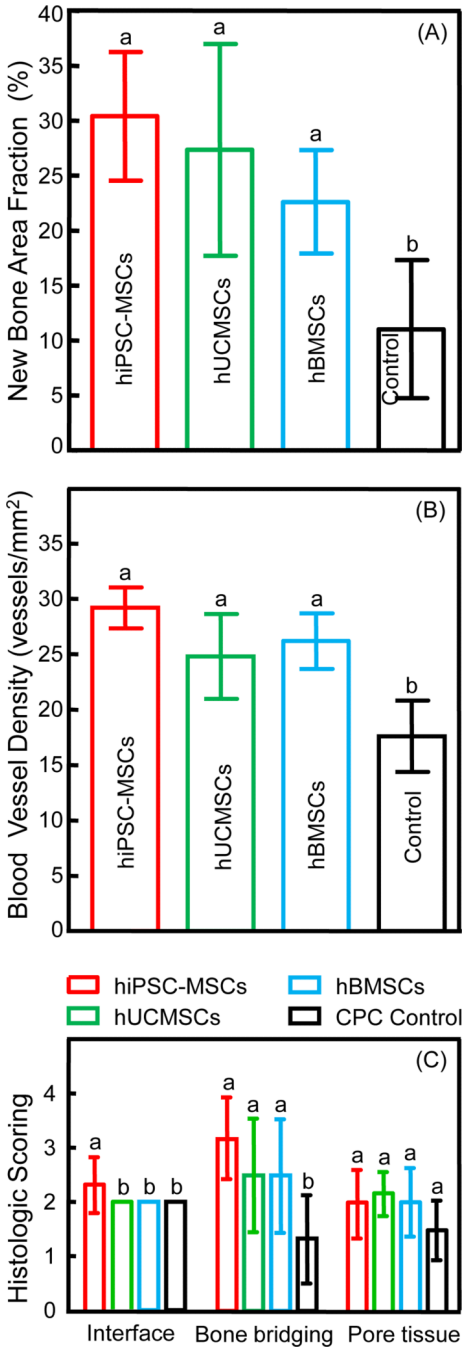

Figure 7.

Histomorphometry analysis of new bone area fraction (A), and new blood vessel density (B). The new bone area and new blood vessel density of hiPSC-MSCs, hUCMSCs and hBMSCs were higher than CPC control ($p < 0.05$). Histologic scoring for new bone is shown in (C). hiPSC-MSC group had the highest score of hard tissue response at bone-scaffold interface and scoring of bone bridging at the dura side. Each value is mean ± sd (technical replicates n = 6). Dissimilar letters indicate significantly different values ($p < 0.05$).

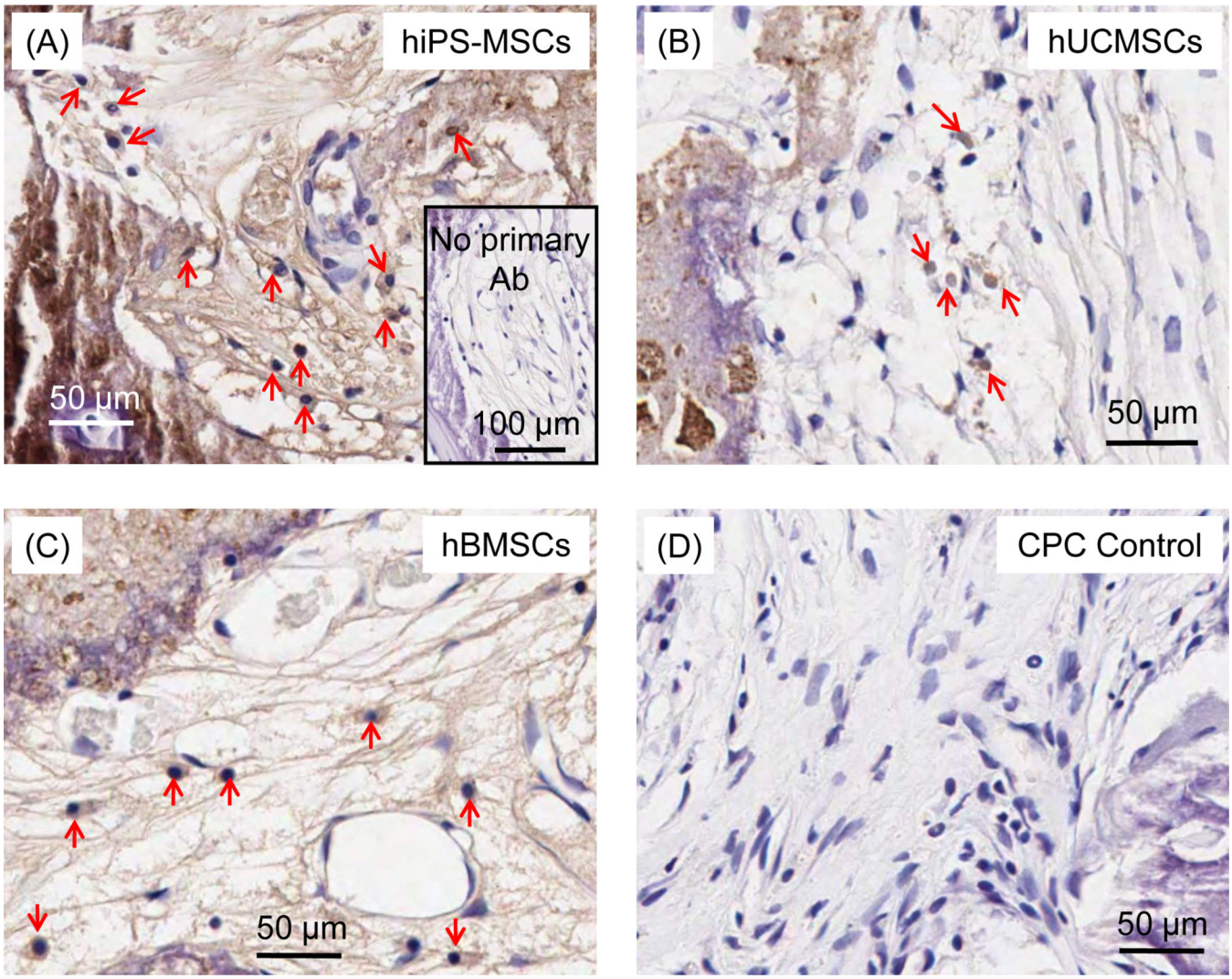

Figure 8.

Immunohistochemical staining for human nuclear antigen 12 w after implantation. hiPS-MSCs (A), hUCMSCs (B), hBMSCs (C), and CPC control (D). The inset in (A) is the negative control without primary antibody incubation. Positive staining (marked by arrows) was mainly found within the non-mineralized fibrous tissue in the pores of the cell-seeded scaffolds. There were no positive areas in CPC control.

Table 1

Histologic scoring for evaluation of new bone formation

Histologic scoring for evaluation of new bone formation	
1. Hard tissue response at bone-scaffold interface	
Direct bone to implant contact without soft interlayer	3
Majority of implant is surrounded by fibrous tissue capsule	2
Unorganized fibrous tissue (majority of tissue is not arranged as capsule)	1
Inflammation marked by an abundance of inflammatory cells and poorly organized tissue	0
2. Bone bridging at the dura side of the defect	
Over 3/4 to the entire length of the defect (≥ 6 mm, ≤ 8 mm)	4
Over 1/2 to 3/4 length of the defect (≥ 4 mm,< 6 mm)	3
Over 1/4 to 1/2 length of the defect (≥ 2 mm,< 4 mm)	2
Only at the defect borders (< 2 mm)	1
None	0
3. Bone formation within the scaffold pores	
Tissue in pores is mostly bone	3
Tissue in pores consists of some bone within mature, fibrous tissue and/ or a few macrophages	2
Tissue in pores is mostly immature fibrous tissue with blood vessels and young fibroblasts invading the space with few macrophages present	1
Tissue in pores consists mostly of inflammatory cells or empty	0